Quasistationary states in the self-gravitating sheet model

Michael Joyce[1,2] and Tirawut Worrakitpoonpon[1]

[1]*Laboratoire de Physique Nucléaire et Hautes Énergies, Université Pierre et Marie Curie, Paris 6, CNRS IN2P3 UMR 7585, 4 Place Jussieu, F-75752 Paris Cedex 05, France*

[2]*Laboratoire de Physique Théorique de la Matière Condensée, Université Pierre et Marie Curie, Paris 6, CNRS UMR 7600, 4 Place Jussieu, F-75752 Paris Cedex 05, France*

(Received 23 December 2010; published 25 July 2011)

We study quasistationary states (QSSs) resulting from violent relaxation in the one-dimensional self-gravitating "sheet model," revisiting in particular the question of the adequacy of the theory of Lynden-Bell (LB) to describe them. For "waterbag" initial conditions characterized by a single phase-space density, the prediction of this theory is, in this model, a function of only one parameter, which can conveniently be chosen to be the ratio of the energy to that in the degenerate limit. Studying a class of such initial conditions in which the shape of the initial waterbag is varied, we find that the LB predictions are reasonably good always in the low-energy region, while at higher energies (i.e., in the nondegenerate limit) they are generally not even qualitatively correct, although certain initial conditions can still be found where they are as good as at low energy. We find notably that, in line with what has been observed by Levin *et al.* in some other models, when LB theory does not work, the QSSs are always characterized by the presence of a *degenerate* core, which these authors explain as the result of dynamical resonances. In short, LB theory appears to be a good approximation only when violent relaxation is sufficiently "gentle," and otherwise a degenerate core-halo structure results.

DOI: 10.1103/PhysRevE.84.011139 PACS number(s): 05.20.−y, 05.45.−a

I. INTRODUCTION

The rich statistical mechanics of long-range interacting systems has been a subject of active study in recent years (for a recent review see, e.g., Ref. [1]). As for self-gravitating systems, such systems have been understood to give rise generically to nonequilibrium states that evolve only on time scales that diverge with the number of particles. The degree to which such "quasistationary" states (QSSs) can be understood, and their properties predicted, by a statistical approach is a question that is inevitably posed. In this context a theory originally formulated by Lynden-Bell in the astrophysical context in the sixties [2], and that has been applied also in the study of two-dimensional (2D) vortices [3], has seen revived interest in recent years. Study notably of a one-dimensional (1D) toy model, the Hamiltonian Mean Field (HMF) model, which describes particles on a ring interacting by a cosine potential, showed that this theory can predict sometimes very accurately the properties of these states (see, e.g., Refs. [4,5] and references therein) and more generally manages to capture the qualitative dependence of the QSSs on initial conditions. While it is clear that the "LB theory" is not entirely adequate in general, these studies suggest that the basic physical principle behind it—maximization of an entropy subjected to the constraints appropriate to Vlasov dynamics—is, at the very least, a reference point for understanding the out-of-equilibrium dynamics of these systems. This contrasts strongly with the view of this theory in the (original) context of the astrophysical literature, where it has simply been discarded as a completely inadequate, and basically irrelevant, theory [6,7]. One recent study [8] of three-dimensional (3D) self-gravitating systems concludes, however, that LB theory may indeed be relevant also to this case. This study shows that in a certain limited range of initial conditions the LB theory predicts well the density profiles of QSSs and proposes an alternative theory to explain their properties in the regime where the LB theory no longer works well. The same authors have shown that the same statements apply both to plasma systems [9] and to a 2D self-gravitating system [10] and, in a very recent article [11], have used the alternative theory to account for QSSs in the HMF model.

In this paper we study these issues in the so-called self-gravitating "sheet model" (SGS) of particles in one dimension attracted by forces independent of separation. Our main goal is to characterize more precisely than has been done previously the degree of validity of the LB theory in this model, which is one of the canonical toy models for the study of such systems, and to determine whether the properties of the QSSs can be characterized in a simple manner and perhaps understood when the LB theory does not apply. That this theory does not provide an adequate theory of QSSs in the SGS model is clear from the earliest studies of this issue [12–14], which indeed used this model to probe the possible validity of LB theory for 3D gravitating systems. More recently a study of these questions in the SGS model has been reported by Yamaguchi [15], who finds reasonable agreement with LB theory in a certain range of initial conditions, and, like in the work of Levin *et al.* mentioned above, proposes a modification of it to account for the QSSs observed in other cases. We will compare in detail our results to these previous works.

Studies of the SGS model in the astrophysical context go back at least as far as that of Ref. [16], and there have been numerous studies of it also in the statistical mechanics literature in the decades since. Many of these studies focused on the question of relaxation to the thermal equilibrium of the model, for which the exact expression was first derived by Rybicki [17]. That this relaxation, like in other long-range systems, takes place very slowly, on a time scale that diverges with the number of particles, has been clear since the earliest studies, but the precise time scale and parametric dependences thereof have been the subject of considerable

study and even some controversy (see, e.g., Refs. [18–21] and references therein). In a recent work [21] on this question, we have established clearly that the relaxation time from a range of initial conditions depends *linearly* on the number of particles N,[1] while also showing a strong dependence on the intermediate QSS state (or states). Besides the early and more recent studies cited above that consider the QSSs attained on the shorter mean-field time scales (i.e., through violent relaxation) and LB theory, there are also studies [24,25] that argue that the assumption that QSSs always result from mean-field dynamics may not be always correct: Starting from certain initial conditions the initial phase of relaxation is observed to lead to phase-space densities that have large holes that rotate in phase space, which persist on the time scales of the simulations. In our analysis below we will examine this question carefully, as it is clearly of central importance to understand whether the formation of a QSS is indeed a good description of the outcome of violent relaxation if one is comparing with a theory that, by construction, assumes such a outcome.

The article is organized as follows. First, we will start in Sec. II with the definition of the model, and its numerical integration. In Sec. III we review the theory of violent relaxation of Lynden-Bell and describe our calculations of the predictions for the density profiles and velocity and energy distributions. We will also introduce a simple set of "order parameters" that we use to characterize the QSSs. In Sec. IV we describe the specific class of initial conditions that we investigate. In Sec. V we report our numerical results, comparing them to the theoretical LB predictions. In the following section we confront our results with two proposals that have been made in the recent literature to explain the properties of QSSs when the LB is clearly inadequate. We also discuss our results briefly in the light of the kinetic theory for collisionless relaxation developed in Ref. [26] (and references therein). In our conclusions we summarize our findings and conclusions and suggest some directions for further investigation in both 1D and 3D self-gravitating systems.

II. THE SELF-GRAVITATING SHEET MODEL

We consider identical particles of mass m in one dimension that are mutually attracted by a force independent of their separation; i.e., the force on a particle i due to a particle j is

$$F_{ij} = -gm^2 \frac{x_i - x_j}{|x_i - x_j|} \equiv -gm^2 \mathrm{sgn}(x_i - x_j),$$

where g is a coupling constant. If the particles in one dimension are considered as infinitely thin parallel sheets in three dimensions interacting by 3D Newtonian gravity, it is simple to show that $gm \equiv 2\pi\Sigma G$, where G is Newton's constant and Σ is the mass per unit surface area of the sheets. In a system of a finite number of such particles the total force acting on the ith particle at any time may be expressed as

$$F_i = gm^2[N_+^i - N_-^i], \tag{1}$$

where N_+^i denotes the number of particles on the right of ith particle and N_-^i for the left.

The fact that the force is thus constant other than when particles cross leads to one of the very nice features of this toy model: Its numerical integration requires only the solution of algebraic (quadratic) equations to determine the time of the next particle crossing. This means that the only limit on the precision of integration is that of the machine in solving such equations, and that no numerical parameters need be introduced. Another simplification comes from the fact that, in one dimension, the crossing of two particles without discontinuity in the velocities is, up to labeling of the particles, equivalent to an elastic collision in which particles exchange velocities. If we are not interested in following the trajectories of individual particles, we can thus consider the system as consisting of particles on which the forces are constant in time [and given by the initial value of (1)], and that undergo elastic collisions when they collide. The optimal way to treat this kind of problem is, as has been pointed out and discussed in detail in Ref. [27], by using a so-called heap-based algorithm, which uses an object called a "heap" to store in an ordered way the next crossing times of the pairs. This algorithm requires a number of operations of order $\log(N)$ to determine which of the $N-1$ pairs crosses next. Given that the number of crossings per particle per unit time grows in proportion to N, the simulation time thus grows in proportion to $N^2\log(N)$. As is common practice we will use the total energy (which is conserved in the continuum model) as a control parameter. For the longest simulations we report the error in total energy of the order of $10^{-9}\%$.

III. PREDICTIONS OF LYNDEN-BELL THEORY

In this section we very briefly recall the basics of the theory of Lynden-Bell and describe how we calculate its predictions for different quantities, in the case of waterbag initial conditions.

A statistical theory to describe the stationary states arising from violent relaxation through mean-field forces was proposed by Lynden-Bell in 1967 [2]. Such states were proposed to arise from the relaxation of the coarse-grained phase-space density to that derived by maximizing the entropy derived for the latter by "counting" the (fine-grained or "microscopic") phase-space configurations states consistent with the conservation laws imposed by the collisionless (Vlasov) dynamics. For the case of an initial "waterbag" phase-space density, i.e., in which the microscopic phase-space density has the same value everywhere it is nonzero, these conservation laws simply require the conservation of the phase-space volume "occupied" by this constant density, e.g., f_0. The calculation of the entropy is then equivalent to that for identical particles with a "fermionic" exclusion and gives (in one dimension)

$$S[\bar{n}] = \iint [\bar{n}\ln\bar{n} + (1-\bar{n})\ln(1-\bar{n})]\,dx\,dv, \tag{2}$$

[1]This result is consistent, notably, with the analysis of Ref. [22], which argues that a time scale linear in N arises because of "resonances" present in spatially inhomogeneous QSSs in 1D systems, but not in spatially homogeneous QSSs that occur in 1D systems such as the HMF model, where a faster scaling with N is indeed observed (see, e.g., Ref. [23]).

where $\bar{n} \equiv \bar{f}/f_0$, and $\bar{f}$ is the coarse-grained phase-space distribution in the macrocell at (x,v). Maximization of (2) gives

$$\bar{f}(x,v) = \frac{f_0}{1 + e^{\beta(\epsilon(x,v)-\mu)}}, \tag{3}$$

where $\epsilon(x,v) = \frac{v^2}{2} + \varphi(x)$ denotes the energy density of phase-space element at (x,v). The constants β and μ are Lagrange multipliers associated with the conservation of the total mass M and total energy E of the system:

$$M = \iint \bar{f}(x,v)\, dx\, dv. \tag{4}$$

$$E = \iint \left(\frac{v^2}{2} + \frac{\varphi}{2}\right) \bar{f}(x,v)\, dx\, d, \tag{5}$$

where $\varphi(x)$ is the mean field potential generated by the mass density $\rho(x)$. Except in the degenerate and nondegenerate limits, corresponding to $\beta \to \infty$ and $\beta \to 0$, respectively, it is not possible to solve these equations analytically to derive (β,μ) for any given M, E, and f_0. It is, however, straightforward to do so numerically, as described in Appendix A (see also Ref. [14]).

We note that, although the prediction of LB theory for a waterbag initial condition depends in general on the three parameters M, E, and f_0, for the SGS model there is only one additional dimensional quantity relevant in the continuum limit, the coupling g. Thus units can always be chosen so that two of M, E, and f_0 are fixed, and the LB prediction can therefore depend nontrivially (up to a rescaling) only on *one parameter*. A convenient choice of this parameter, which we will use here, is

$$\xi_D \equiv \frac{E - E_D}{E_D}, \tag{6}$$

where $E_D(M, f_0)$ is the energy of the system with mass M and phase-space density f_0 in the degenerate limit; i.e., ξ_D is the energy of the system above the degenerate limit normalized to the lowest energy possible for the same mass and phase-space density. The expression for E_D is given in Appendix B (see also Ref. [14]).

We next describe how we derive, once β and μ are known, the LB predictions for the various quantities we will measure in our simulations.

A. Spatial distribution

Using (3), the Poisson equation gives

$$\frac{\partial^2\varphi(x)}{\partial x} = 2g\rho(x) \equiv 2g \int_{-\infty}^{\infty} \frac{f_0}{1 + e^{\beta\left[\frac{v^2}{2}+\varphi(x)-\mu\right]}}\, dv, \tag{7}$$

where $\rho(x)$ is the mass density profile (which we will refer to simply as the "density profile"). It is simple numerically to solve this (second-order differential) equation for $\varphi(x)$, and then to determine the mass density profile, using the boundary conditions $\frac{d\varphi}{dx}|_{x=0} = 0$ and $\varphi|_{x=0} = 0$.

B. Velocity distribution

The velocity distribution may be written

$$\theta(v) = 2\int_0^{\infty} \frac{f_0}{1 + e^{\beta\left(\frac{v^2}{2}+\varphi-\mu\right)}} \frac{1}{a(\varphi)}\, d\varphi, \tag{8}$$

where

$$a(x) = \frac{\partial\varphi(x)}{\partial x} \tag{9}$$

is, up to a sign, the gravitational acceleration. Using the Poisson equation we have

$$\frac{d^2\varphi(x)}{dx^2} = \frac{1}{2}\frac{\partial[a^2(\varphi)]}{\partial\varphi} = 2g\rho, \tag{10}$$

and therefore

$$a(\varphi) = \sqrt{4g\int_0^{\varphi} \rho(\varphi')\, d\varphi'}. \tag{11}$$

Using the previously determined $\rho(\varphi)$ we obtain $\theta(v)$ using (8).

C. Energy distribution

The distribution of particle energies is defined by

$$F(\epsilon) = \int \delta\left\{\epsilon - \left[\frac{v^2}{2} - \varphi(x)\right]\right\} \bar{f}(x,v)\, dx\, dv \tag{12}$$

with

$$\int F(\epsilon)\, d\epsilon = 1. \tag{13}$$

Integrating we obtain

$$F(\epsilon) = D(\epsilon)\bar{f}(\epsilon), \tag{14}$$

where

$$D(\epsilon) = \int_0^{\epsilon} \frac{1}{a(\varphi)} \frac{2\sqrt{2}}{\sqrt{\epsilon - \varphi}}\, d\varphi \tag{15}$$

is the density of states at energy ϵ.

While the results for $\rho(x)$ and $\theta(v)$ do not depend on the choice of the zero point of the potential, this latter result does. It is straightforward, numerically, to use, rather than $\varphi|_{x=0} = 0$,

$$\varphi_0 \equiv \varphi|_{x=0} = g\int_{-\infty}^{\infty} |x|\rho(x)\, dx, \tag{16}$$

i.e., that corresponding to a pair potential strictly proportional to the separation between particles. Given that $a(x)$ defined in (9) is necessarily positive for all $x \neq 0$, this is the minimum value of the potential (and of the energy particle energy). Adapting this definition the energy distribution is still given by (14), but with $D(\epsilon) = 0$ for $\epsilon < \varphi_0$ and

$$D(\epsilon) = \int_{\varphi_0}^{\epsilon} \frac{1}{a(\varphi)} \frac{2\sqrt{2}}{\sqrt{\epsilon - \varphi}}\, d\varphi. \tag{17}$$

D. Order parameters

In order to characterize and compare the macroscopic properties of QSSs it is convenient to calculate specific moments of the phase-space distribution (rather than to study always the full distribution). As discussed in Ref. [21] a particularly relevant choice can be normalized "crossed moments" which give a measure of the "entanglement" of the distribution in space and velocity coordinates, by considering

$$\phi_{\alpha\beta} = \frac{\langle |x|^\alpha |v|^\beta \rangle}{\langle |x|^\alpha \rangle \langle |v|^\beta \rangle} - 1 \tag{18}$$

for nonzero α and β, where

$$\langle u \rangle \equiv \frac{\iint u f(x,v)\, dx\, dv}{\iint f(x,v)\, dx\, dv} \tag{19}$$

estimated in the discrete system with N particles as

$$\langle u \rangle \equiv \frac{1}{N} \sum_{i=1}^{N} u_i, \tag{20}$$

where u_i is the value measured for the particle i. In thermal equilibrium the distribution function is separable, and so $\phi_{\alpha\beta} = 0$. Further it can be shown easily [21] that the thermal equilibrium solution at any energy is the unique separable stationary state; i.e., all QSSs are nonseparable. Thus generically we expect these moments to be nonzero in a QSS (although any finite number of them can in principle vanish without implying separability).

Here we will use specifically the two moments ϕ_{11} and ϕ_{22} to characterize and compare the QSSs we obtain in our numerical simulations, complemented when necessary by examination of the functions derived above and in some cases of the full phase-space density. Given the LB solutions determined above (for waterbag initial conditions) it is straightforward to calculate numerically the values of ϕ_{11} and ϕ_{22} predicted by LB for this case. These are shown in Fig. 1 as a function of the parameter ξ_D (which, as discussed above, can be taken as the single parameter on which the LB result depends). We note that both parameters are always negative but increase toward zero as we go to the nondegenerate limit. Indeed in this limit the LB prediction tends to the (separable) thermal equilibrium solution.

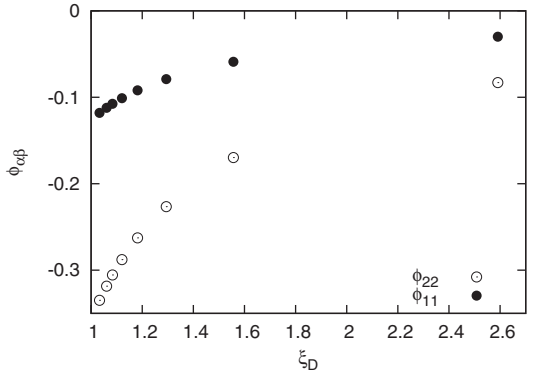

FIG. 1. The "order parameters" ϕ_{11} and ϕ_{22} of the QSSs predicted by LB theory for waterbag initial conditions, plotted as a function of the normalized energy ξ_D.

IV. INITIAL CONDITIONS

In our numerical study we consider particles distributed initially by randomly sampling different classes of waterbag initial conditions, i.e., in which the phase-space density takes the same value f_0 everywhere it is nonzero. Specifically we consider, in order:

(1) *Single rectangular waterbags (SRWs)*, in which the support of the initial phase-space density is a rectangle centered on the origin, i.e.,

$$f(x,v) = f_0 \Theta(x_0 - x)\Theta(x_0 + x)\Theta(v_0 - v)\Theta(v_0 + v), \tag{21}$$

where Θ is the Heaviside function. As, in the continuum limit, the only parameters in the problem are then four—f_0, x_0, v_0, and the coupling g—there is in fact only one relevant parameter characterizing the system once units are chosen. A natural physical choice of this parameter is the initial virial ratio R_0, which a simple calculation shows is given by

$$R_0 \equiv \frac{2T_0}{U_0} = \frac{v_0^2}{gMx_0}, \tag{22}$$

where T_0 and U_0 are the initial kinetic and potential energies given by

$$T_0 = \tfrac{1}{6} M v_0^2, \quad U_0 = \tfrac{1}{3} g M^2 x_0. \tag{23}$$

An example of such a configuration with $R_0 = 0.5$ is given in the left panel of Fig. 2. As discussed above the LB prediction also depends on only one parameter, which we can take to be ξ_D, the ratio of the energy of the configuration to that of the degenerate limit of LB (i.e., the minimum allowed energy of the given mass at phase-space density f_0). The energy and mass in the limit of a degenerate system are given as functions of μ by (B5) and (B4). Eliminating μ we obtain

$$E_D = \frac{B\left(\frac{3}{2},\frac{2}{3}\right)}{12^{\frac{1}{3}}} g x_0 M^2 R_0^{\frac{1}{3}}, \tag{24}$$

and thus

$$\xi_D = \frac{E}{E_D} = \frac{12^{\frac{1}{3}}}{3B\left(\frac{3}{2},\frac{2}{3}\right)} \left(\frac{1}{R_0^{\frac{1}{3}}} + \frac{R_0^{\frac{2}{3}}}{2} \right) = 0.688 \left(\frac{1}{R_0^{\frac{1}{3}}} + \frac{R_0^{\frac{2}{3}}}{2} \right) - 1, \tag{25}$$

where $B(\frac{3}{2},\frac{2}{3})$ is a beta function. This expression is is plotted in Fig. 3. The SRW with $R_0 = 1$ is thus the lowest energy configuration, and there are otherwise two values of R_0 for each value of ξ_D.

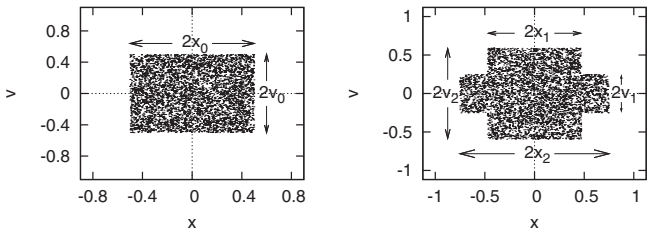

FIG. 2. Realizations with $N = 5000$ particles of an SRW initial condition (left panel) and DRW initial condition (right panel). The two configurations have the same value of ξ_D (up to finite N corrections). The units used here are specified at the beginning of Sec. V.

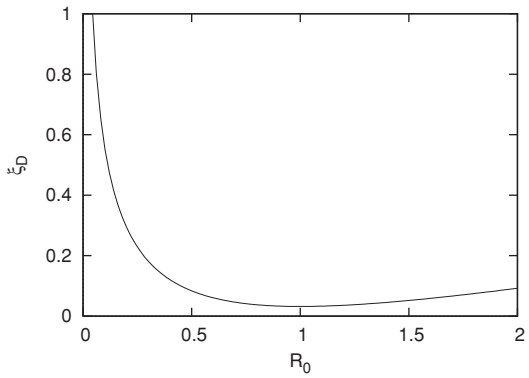

FIG. 3. ξ_D as a function of R_0 for an SRW initial condition.

(2) *Double rectangular waterbags (DRWs)*, in which the support of the initial continuum phase-space density is like that shown in the right panel of Fig. 2:

$$f(x,v) = f_0\Theta(x+x_1)\Theta(x_1-x)\Theta(v+v_1)\Theta(v_1-v) + f_0\Theta(x+x_2)\Theta(-x_1-x)\Theta(v+v_2)\Theta(v_2-v) + f_0\Theta(x-x_2)\Theta(x_1-x)\Theta(v+v_2)\Theta(v_2-v).$$

As this has two additional parameters compared to the SRW, it is effectively a *three* parameter family of initial conditions, which coincides with the SRW when $v_1 = v_2$, $x_1 = 0$ or $x_1 = x_2$. When they differ from the SRWs, they are spatially inhomogeneous, with a ratio of densities $\delta = \frac{v_1}{v_2}$ in the two different regions. We will choose to characterize them by this parameter, together with ξ_D and the initial virial ratio R_0. LB theory thus predicts that the final state should be independent of R_0 and δ at given ξ_D. The relevant expressions for the kinetic and potential energies of the DRW configuration are given in Appendix C.

(3) *Disjoint waterbags (DWs)*, in which the initial phase-space density is made of two disjoint regions with simple shapes, either rectangular or elliptical. We will use such configurations to further explore some of the conclusions draw from the study of the SRW and DRW configurations.

V. NUMERICAL RESULTS

A. Choice of units

Unless otherwise indicated our results will be given in units fixed by taking $g = 1, M = 1$, and $L_0 = 1$ where L_0 the *initial linear size of the system*, i.e., the distance between the outer extremities of the theoretical waterbag initial condition. This implies that the unit of time is

$$t_c = \frac{1}{\sqrt{g\rho_0}}, \tag{26}$$

where $\rho_0 = M/L_0$ is the initial mean mass density. This is simply a characteristic time scale for a particle to cross the system. In the cold limit (i.e., with zero initial velocity, with $R_0 \to 0$) of the SRW initial conditions, it corresponds exactly to the time in which all the mass falls to the center of the system.

B. Attainment of QSSs and their characterization: generalities

That the SGS model with a large number of particles—just as such 3D self-gravitating and other long-range interacting systems which have been studied in the literature—give rise typically to QSSs starting from initial conditions such as those above has been discussed elsewhere in many studies (see references given in the introduction). The attainment of a QSS should be tested, in theory, by considering the full phase-space density coarse-grained at some chosen scale. One would then verify whether its evolution after some initial period (of violent relaxation) tends to

$$\bar{f}(x,v,t) = \bar{f}_{QSS}(x,v) + \delta\bar{f}(x,v,t), \tag{27}$$

where the amplitude of the fluctuations $|\delta\bar{f}(x,v,t)|$ decreases as N increases. For our study here, in which we consider how the properties of these QSSs depend on the initial conditions, what is of importance is that we evolve the corresponding system to a time at which the approximation (27) indeed holds well, for N sufficiently large so that the fluctuations $\delta\bar{f}(x,v,t)$ introduce a negligible uncertainty into the quantities used to characterize the QSSs.

In practice numerical limitations on N make a direct analysis extremely difficult, and one typically considers the behavior of single macroscopic parameters, such as the virial ratio, or the magnetization in models (e.g., the HMF model) where it is defined. This is then complemented by a visual inspection of the system represented in phase space. To describe the properties of the QSS one then considers typically the density profiles, velocity and/or energy distribution. We have shown in Ref. [21], where we studied the very long time behavior of QSSs resulting from SRW initial conditions, that the parameters ϕ_{11} and ϕ_{22} defined above are very useful macroscopic "order parameters," which can be used to diagnose both the attainment of a QSS and to characterize this state. We will use them here for the same purpose, supplementing their calculation where necessary, or interesting, by a fuller analysis of the distribution functions.

To determine whether a QSS is reached, and on what time scale, we thus study first the evolution of the virial ratio and of ϕ_{11} and ϕ_{22}. While the characteristic time for the mean-field dynamics is of order t_c defined above, the completion of relaxation to QSSs (in the sense defined above) takes typically of order several tens to one hundred t_c for SRW initial conditions. Further, this time depends, unsurprisingly, on the nature of the initial condition, with very cold initial conditions—further from virial equilibrium initially—taking significantly longer to relax.

For DRW and DW initial conditions we observe even greater variation in the time for full relaxation to a QSS than for SRW, with, in some cases, significant persistent fluctuations in the macroscopic parameters. An example of such a case is shown in Fig. 4, in which the upper panel shows the evolution of the virial ratio and the lower panel that of the parameters ϕ_{11} and ϕ_{22}, for a DW initial condition sampled with $N = 10^4$ particles. The full phase-space plot is shown in Fig. 5. This reveals that it is a persistent "rotating hole" feature in the phase space, which gives rise to the (small but clearly visible) coherent fluctuations in the

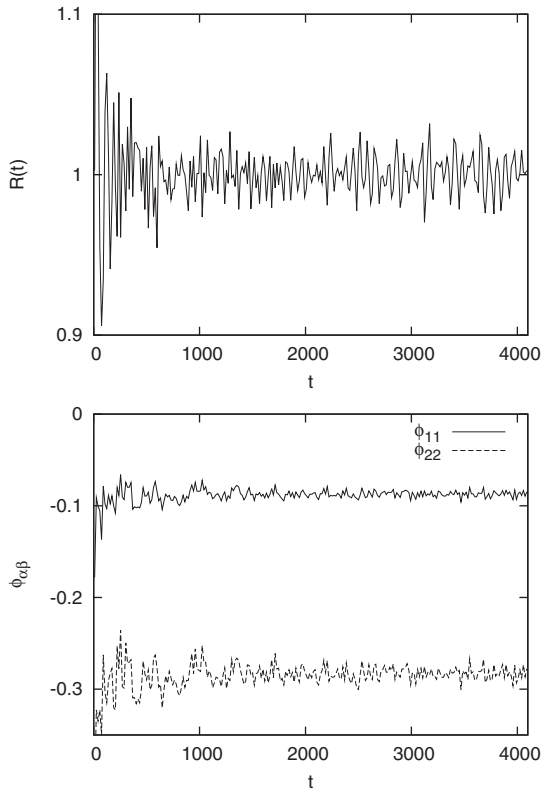

FIG. 4. Temporal evolution of virial ratio (top) and ϕ_{11} and ϕ_{22} (lower) starting from a realization with $N = 10^4$ particles of a DW initial condition (shown in first panel of Fig. 5). The time units here are such that $t_c = \sqrt{3/2}$, i.e., $t = 10 \approx 8.2t_c$.

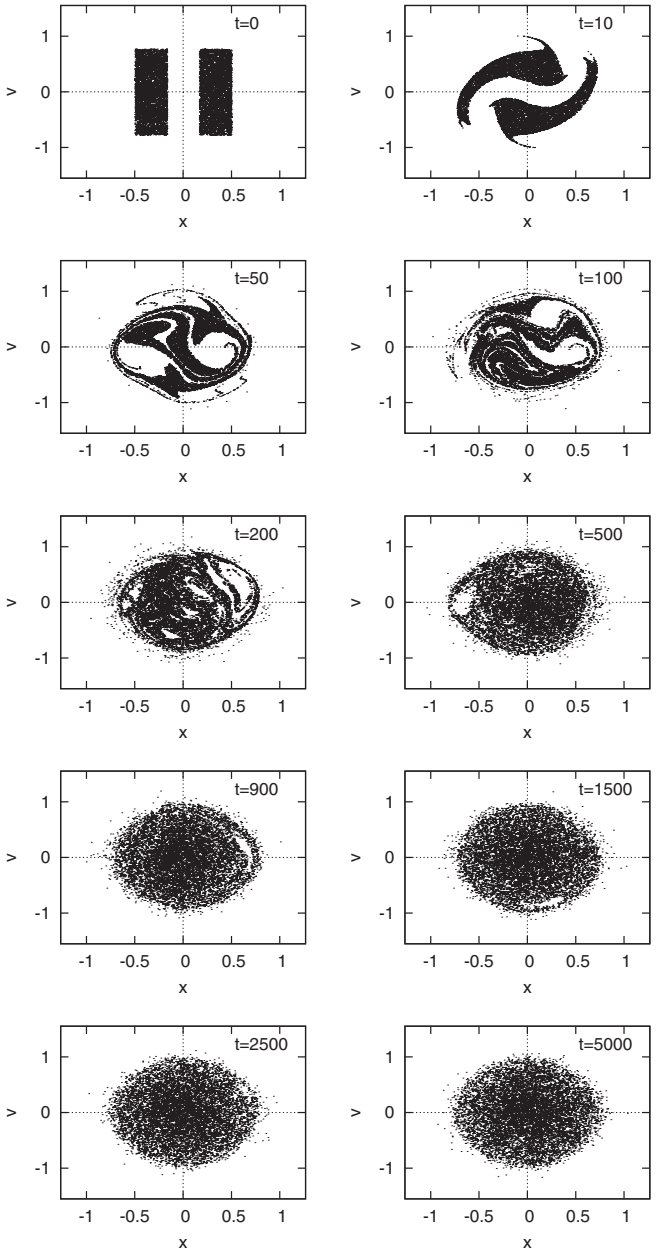

FIG. 5. Phase-space plot of particle trajectories evolved from the DW initial condition shown in the first panel (with $N = 10^4$ particles). The time units are those indicated in the previous figure.

averaged parameters in Fig. 4. This is precisely the kind of effect that has been documented in the two studies [24,25] mentioned in the introduction, and that has been argued in this context to show that LB theory is incorrect (as it predicts, by construction, the attainment of a time-independent phase-space density). While the hole we observe is clearly visible at $t = 500$ and indeed rotates in phase space, the subsequent two panels show that it slowly disappears on a time scale of order a few thousand dynamical times. Thus it appears that the relaxation of these holes simply represents a prolongation of the *collisionless* relaxation to a well-defined QSS, as no tendency of the system to evolve toward thermal equilibrium (corresponding to ϕ_{11} and ϕ_{22} equal to zero) is evidenced on this time scale. Further study, however, would be required to establish this conclusion more definitively for a broader range of initial conditions, and to exclude notably that collisional relaxation may play some role.

C. SRW initial conditions

The density profiles, velocity distributions, and energy distributions in the QSSs obtained starting from SRW configurations with $R_0 = 0.1, 0.5, 1$ are shown in Figs. 6, 7, and 8. These correspond to averages over 30 realizations of each initial condition sampled with $N = 5000$ particles, taken at $t = 200t_c$, by which time the QSS is well established. In each case the LB predictions given in Sec. III are shown also, corresponding to $\xi_D = 0.56, 0.08,$ and 0.03, respectively. As observed already in early studies [13,14] the qualitatively most striking deviation from the prediction of LB theory is marked by the appearance of a "core-halo" structure, most clearly evident in the energy distribution obtained from the $R_0 = 0.1$ initial condition. On the other hand, as underlined in the more recent study of Ref. [15] for these same initial conditions, the agreement of the LB theory with the observed QSS is in fact quite good for the case $R_0 = 1$, while the discrepancy progressively increases as R_0 deviates from unity and a core-halo-type structure appears.

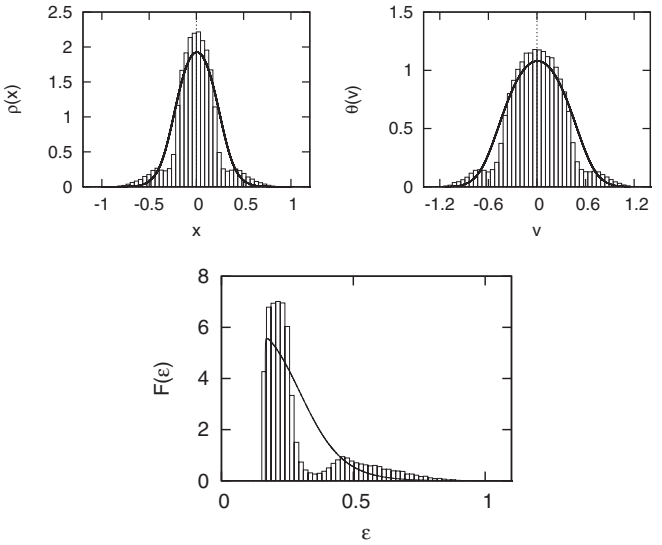

FIG. 6. The density profile (top left), velocity distribution (top right), and energy distribution (bottom) for the QSSs obtained starting from SRW with $R_0 = 0.1$. The solid lines are the corresponding LB predictions.

Shown in Fig. 9 are the values of the parameter ϕ_{11} and ϕ_{22} in the QSS and the values predicted by LB theory. This plot summarizes in a simple manner the conclusions above: the theory works quite well quantitatively at the lowest energy state corresponding to $R_0 = 1$, but deviates greatly as we go toward the less degenerate initial states. Further, the plot shows that the theory gives very qualitatively the correct behavior of the parameters—they increase monotonically with the initial ξ_D. At low degeneracy the sign of these parameters is a result of the formation of a core that is colder than predicted: There is in this case an excess of low-velocity particles at small x.

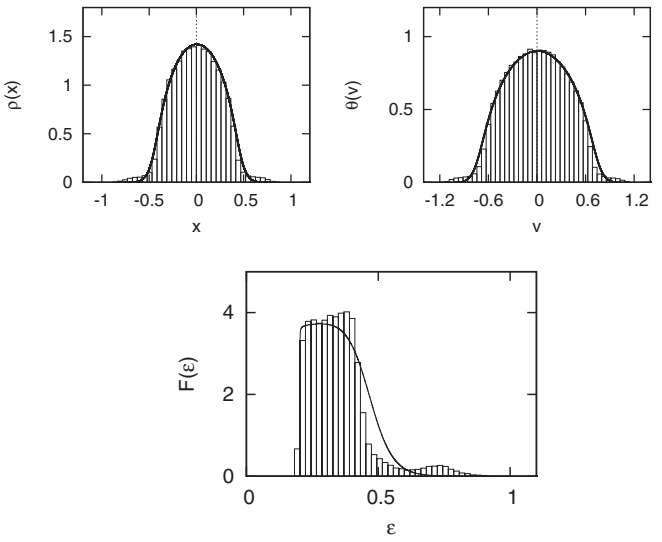

FIG. 7. The density profile (top left), velocity distribution (top right), and energy distribution (bottom) for the QSS obtained starting from SRW with $R_0 = 0.5$. The solid lines are the corresponding LB predictions.

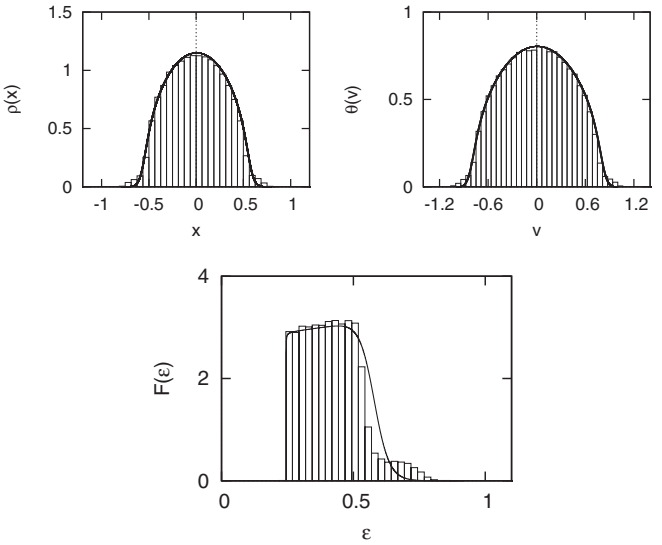

FIG. 8. The density profile (top left), velocity distribution (top right), and energy distribution (bottom) for the QSS obtained starting from SRW with $R_0 = 1$. The solid lines are the corresponding LB predictions.

We note that these single parameters, ϕ_{11} and ϕ_{22}, actually allow a better diagnosis of the closeness to LB theory than the examination of the full density or velocity distribution functions. Indeed, comparing just these two latter functions with the LB predictions, we might conclude that the agreement is almost perfect. The energy distribution, on the other hand,

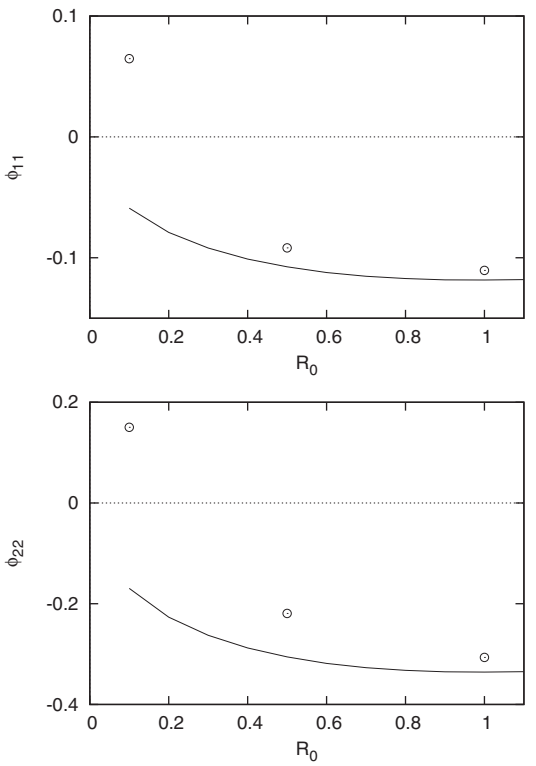

FIG. 9. ϕ_{11} (top) and ϕ_{22} (bottom) in QSSs as the function of R_0. The line indicates $\phi_{\alpha\beta}$ calculated by LB stationary state, and the circle is the value obtained by numerical simulation.

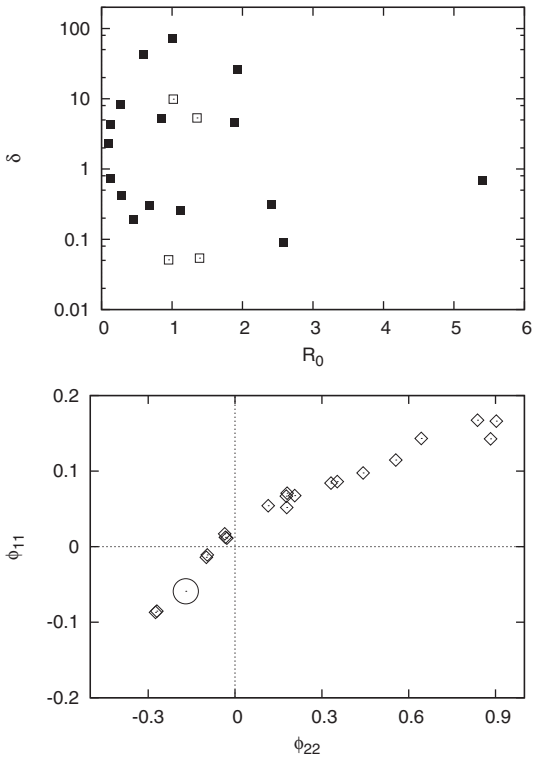

FIG. 10. The upper plot represents the 20 different DRW initial conditions with $\xi_D = 0.56$ (i.e., equal to that of SRW with $R_0 = 0.1$) according to their values of R_0 and δ. The lower plot represents the values of (ϕ_{22},ϕ_{11}) measured in the resulting QSS. The LB prediction lies at the center of the small circle. The unfilled points in the upper plot correspond to the four initial conditions that give QSSs closest to the LB prediction.

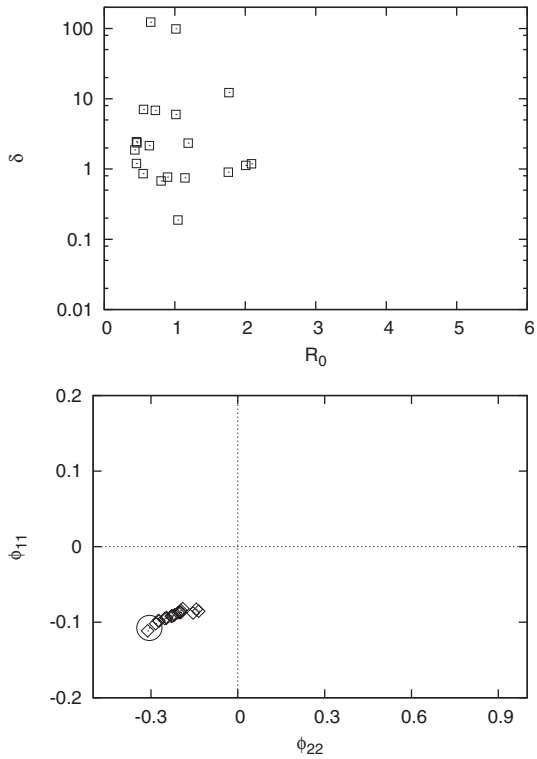

FIG. 11. Same as in Fig. 10, but for DRW initial conditions with $\xi_D = 0.08$, i.e., equal to that of SRW with $R_0 = 0.5$. Scale is as in the previous figure for easier comparison.

allows one to see clearly the discrepancies, which are then reflected well in ϕ_{11} and ϕ_{22}.[2] When considering a larger space of initial conditions, as we do now, it is very convenient to use these parameters as diagnostics of the validity of the LB theory.

D. DRW initial conditions

As described above the DRW initial conditions allow us to test further a basic prediction of LB theory: The same QSS should result starting from any initial configuration in the range of accessible "microstates" at given mass and energy. For 1D gravity and waterbag initial conditions, this means the QSS obtained should be the same at a given ξ_D independently of the shape of the waterbag. As discussed, the DRW gives us a 2D space of such configurations, which we choose to parametrize by the initial virial ratio R_0 and density contrast δ.

For each of the three values of ξ_D corresponding to the SRW initial conditions above, we have simulated 20 different initial conditions chosen to explore the available (R_0, δ) space. In each of Figs. 10, 11, and 12 are shown two plots: One shows the initial conditions in the (R_0, δ) plane at the given value of ξ_D, the other QSSs obtained from them as represented in the plane (ϕ_{11}, ϕ_{22}). The results are, as for the SRW above, averages over 30 realizations of each initial condition sampled with $N = 5000$ particles, taken at $t \approx 200t_c$. The fact that the spread in values of (R_0, δ) is much smaller at smaller ξ_D is simply a reflection of the fact that as one goes toward the degenerate limit $\xi_D = 0$ the constraints limit the possible deformations more and more.

In continuity with what we observed for the SRW, the results show that LB theory works reasonably well at the two lower values of ξ_D—the QSS varies only very little over the range of different initial conditions— and it is grossly violated as we go toward the nondegenerate limit. Indeed, the order parameters for QSSs obtained starting from the same ξ_D can differ in sign. Direct analysis of the distribution functions confirms that this corresponds to QSSs that are completely different. On the other hand, certain initial conditions at $\xi_D = 0.56$—those corresponding to the unfilled points in the upper plot of Fig. 10—do appear to give QSSs close to the LB prediction. To assess whether this is really the case, the density profiles, velocity, and energy distribution functions for two of these are shown in Figs. 13 and 14. While the agreement with the theoretical curves is not perfect, it is comparable with that obtained for the initial conditions with $\xi_D = 0.03$—indeed, the discrepancy between

[2]This "efficiency" of these parameters as diagnostic tools was noted in Ref. [21], where it was shown, notably, that they could identify clearly stationary states arising from certain initial conditions as QSSs rather than the thermal equilibrium states, which previous studies [28] had mistakenly inferred them to be based on an analysis using $\rho(x)$ and $\theta(v)$.

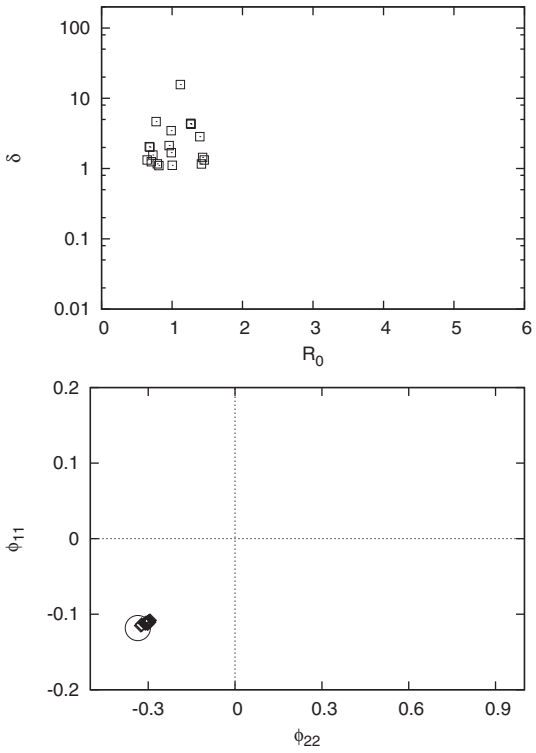

FIG. 12. Same as in Fig. 11, but for DRW initial conditions with $\xi_D = 0.03$, i.e., equal to that of SRW with $R_0 = 1$. Same scale as in Fig. 10 for ease of comparison.

the LB prediction and the observed distributions is no more than observed above for the SRW initial conditions with $\xi_D = 0.03$.

The strong deviations from the LB prediction, just as in the SRW, manifest themselves in the shift toward positive values of ϕ_{11} and ϕ_{22}. Direct inspection of the distribution function of energy shows that this reflects again in all cases

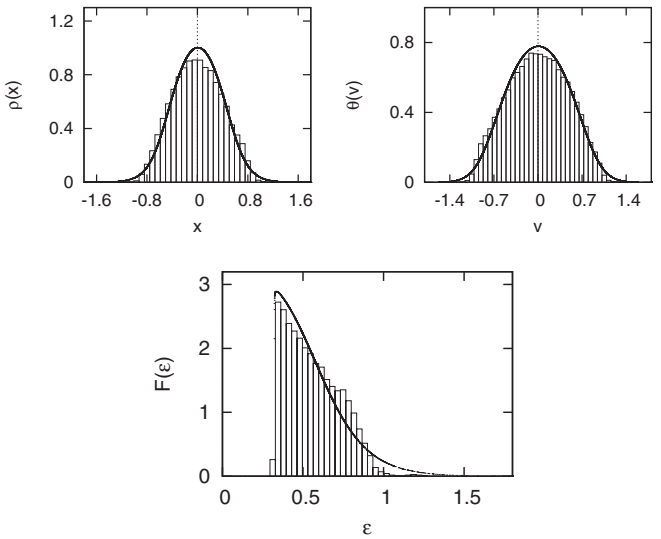

FIG. 13. Density profile (top left), velocity (top right), and energy distribution (bottom) for DRW initial conditions with $\xi_D = 0.56$ (i.e., the same energy as the SRW with $R_0 = 0.1$), $R_0 = 1.39$, and $\delta = 0.054$.

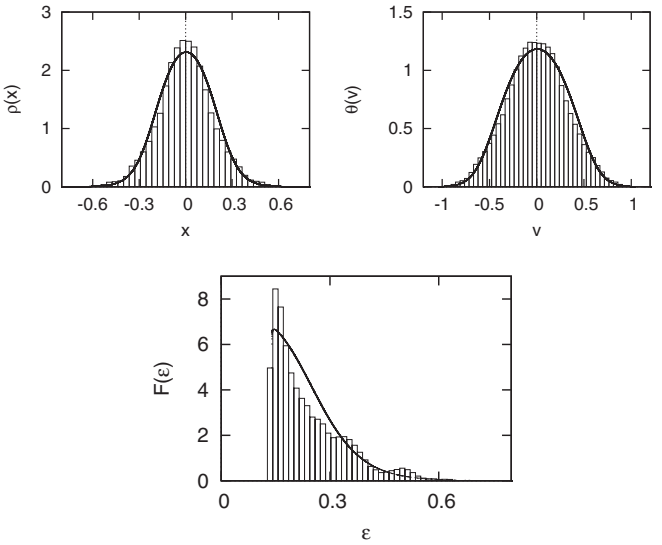

FIG. 14. Density profile (top left), velocity (top right), and energy distribution (bottom) for DRW initial conditions with $\xi_D = 0.56$ (i.e., the same energy as the SRW with $R_0 = 0.1$), $R_0 = 1.017$, and $\delta = 9.861$.

the appearance of a pronounced core-halo-type structure. Inspection of the plot of the initial conditions in the (R_0, δ) space for $\xi_D = 0.56$ shows that all the cases that approach LB (unfilled points) are characterized by an initial virial ratio near unity, while the density contrast parameter δ appears to be irrelevant. On the other hand, $R_0 \approx 1$ is clearly not a sufficient condition to guarantee agreement with LB.

These results suggest therefore that LB theory works reasonably well always near the degenerate limit, and for much higher energies for very specific initial conditions. In these cases, which seem to correlate strongly with an initial virial ratio near unity, the formation of a core-halo structure, not predicted by LB theory, is avoided.

E. DW initial conditions

To further explore these findings, and in particular to investigate the relevance of the initial virial ratio as a parameter, we consider finally a few other "disjoint" waterbag initial conditions as described above. We report results for the four cases shown in Fig. 15. Each of the initial conditions has been adjusted to have $R_0 = 1$, and the values of the normalized energy are $\xi_D = 1.59, 0.58, 0.49$, and 0.23 for DW1 to DW4, respectively. We take in each case a single realization with $N = 10^4$ particles and calculate a time average by sampling on 100 equally spaced time slices in the time window $[4000, 5000]$ (in the time units of our simulation, which differ in each case from units with $t_c = 1$ by a numerical factor of order unity). Shown in Fig. 16 are the QSSs obtained as represented in the (ϕ_{11}, ϕ_{22}) plane. In each case the filled symbol represents the corresponding LB predictions. Compared to the results for SRW and DRW initial conditions, the QSSs appear in all cases much closer to the LB predictions. This is confirmed by inspection of the distribution functions, which are shown for

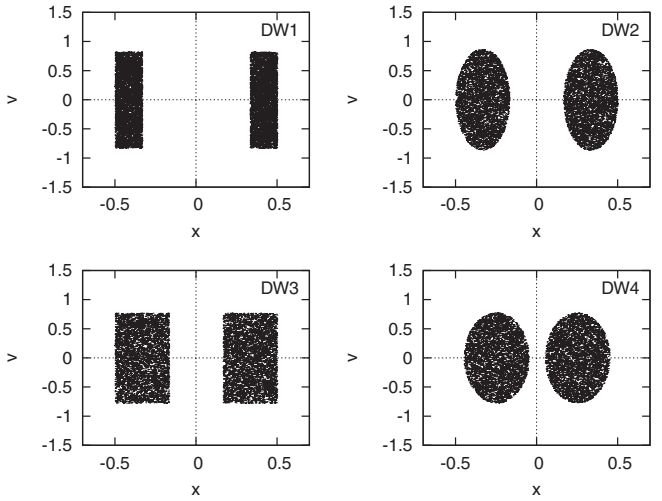

FIG. 15. Four disjoint waterbag initial conditions with the number of case indicated in the panel. The corresponding ξ_D are equal to 1.59,0.58,0.49, and 0.23 for cases 1–4, respectively.

DW2 in Fig. 17 and for DR1 in Fig. 18. For the former case the results are as close to the LB predictions as for the SRW and DRW cases that gave best agreement with LB, with the small deviation being visible again in the energy distribution but very difficult to discern in $\rho(x)$ or $\theta(v)$. The results for the cases DR3 and DR4 are similar. For DR1, on the other hand, the deviation from LB is much more marked, and we see in the energy space that this deviation is associated to the formation of a (in this case very small) core. Very much in line with the results for SRW and DRW initial conditions, the agreement with LB thus deteriorates as one goes away from the degenerate limit.

In summary these results confirm the conclusion drawn from the analysis of the SRW and DRW waterbags: The LB predictions are always reasonably good—and excellent for the spatial and velocity distributions—for (waterbag) initial conditions with low ξ_D, but even at higher values good agreement can be obtained in cases characterized by an initial virial ratio of order unity. Further deviation from LB is always characterized by the appearance of a core-halo-type structure.

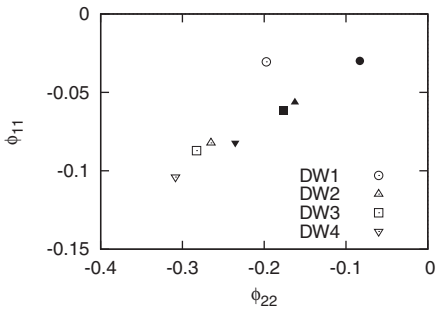

FIG. 16. ϕ_{22} and ϕ_{11} of the QSSs obtained from the initial conditions in the previous figure. The unfilled symbols corresponds to the values obtained from numerical simulations, and the filled symbols are the LB predictions.

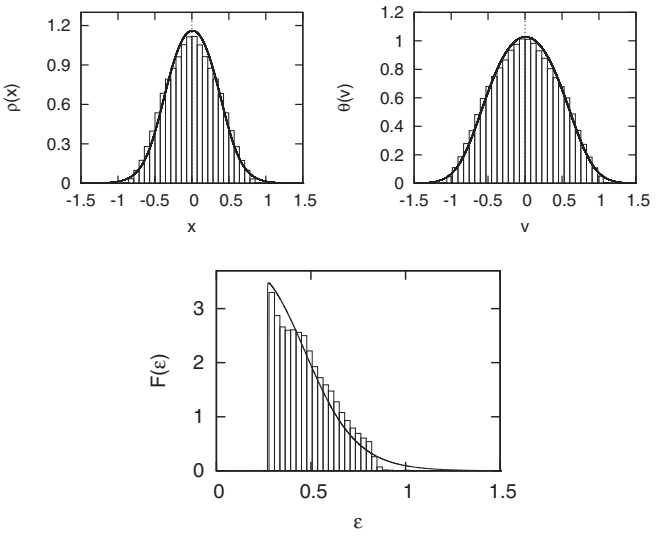

FIG. 17. The density profile (top left), velocity distribution (top right), and energy distribution (bottom) for the QSSs obtained starting from the DW2 initial conditions ($\xi_D = 0.58$). The solid curves lines are the LB predictions.

VI. COMPARISON WITH THEORETICAL PROPOSALS BEYOND LB: DIRECT ANALYSIS OF PHASE-SPACE DENSITY

Let us consider how well two recent proposals in the literature can account for the properties of the QSSs we observe:

(1) Yamaguchi [15] studies the SGS model for SRW initial conditions and notes (as was remarked also in early studies [13,14]) that the breakdown of LB theory is associated with the apperance of a core-halo structure. He proposes a phenomenological adaptation of LB theory which he uses to fit the resultant core, in which the LB theory is applied only to the mass and energy associated to the core. In practice this

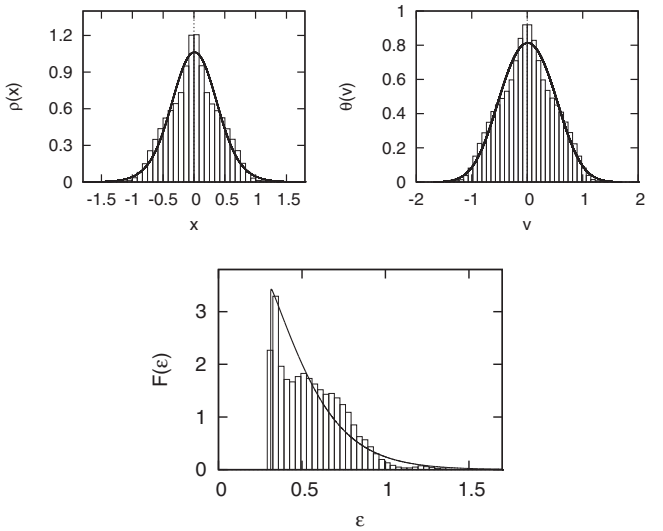

FIG. 18. The density profile (top left), velocity distribution (top right), and energy distribution (bottom) for the QSSs obtained starting from the DW1 initial conditions ($\xi_D = 1.59$). The solid curves lines are the LB predictions.

means that one parameter is measured *a posteriori* from the observed QSSs.

(2) Levin *et al.* in a series of works on other models—plasmas [9], 3D gravity [8], 2D gravity [10], and, most recently, the HMF model [11]—have proposed that, when LB theory breaks down, QSSs correspond to the phase-space density:

$$f(x,v) = f_0[\Theta(e_F - e) + \chi\,\Theta(e - e_F)\Theta(e_h - e)]. \qquad (28)$$

As in the case of Ref. [15], this involves the addition of one parameter compared to LB theory. However, a physical explanation is proposed for the core-halo form of (28), and a prediction for this additional parameter is derived from the initial conditions: An analysis of particle dynamics in the coherent oscillating field associated with the relaxation shows that there are dynamical resonances that allow particles to gain energy, with e_h corresponding to the maximal energy that can be attained in this way. Assuming that resonance effect is "shut off" only by the upper bound on the phase-space density

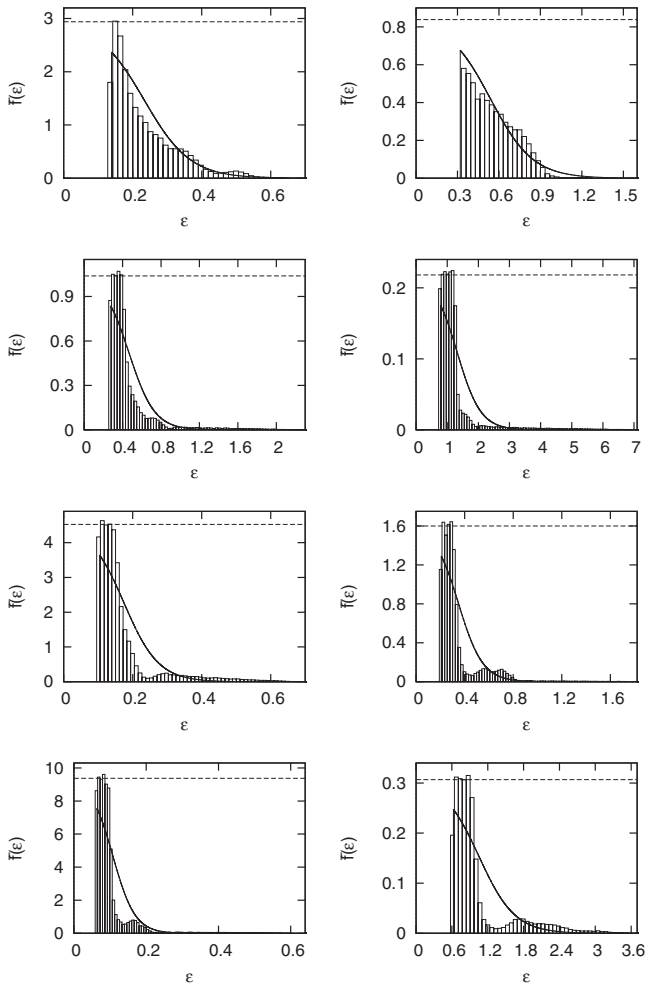

FIG. 19. Phase-space density as a function of energy $\bar{f}(\epsilon)$ for eight representative cases of DRW initial conditions with $\xi_D = 0.56$ (corresponding to $R_0 = 0.1$ for SRW). The two upper panels correspond to the two cases for which the distribution functions are shown in Figs. 13 and 14 where the QSS is close to LB. The dashed horizontal line indicates the initial phase-space density, f_0, and the continuous lines correspond to the LB prediction.

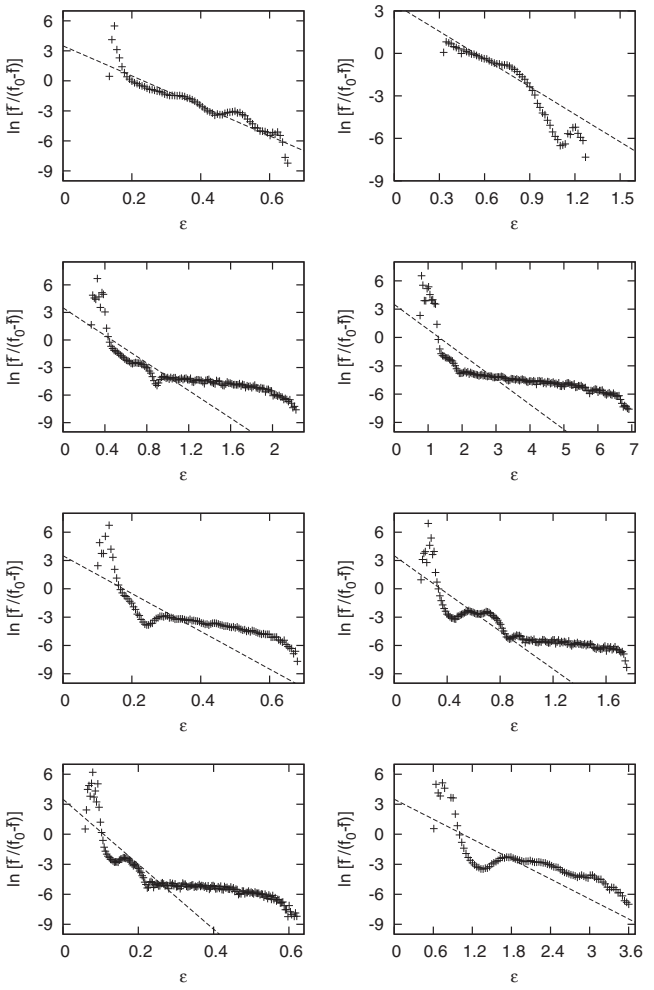

FIG. 20. Exactly the same data as in the previous figure, but now with the logarithm of the absolute value of $\bar{f}/(f_0 - \bar{f})$ plotted as a function of particle energy ϵ. The dashed lines represent the predictions of LB theory (which become straight lines of slope β in this representation).

imposed by the collisionless dynamics, the ansatz (28) is the simplest one possible for the QSSs that will result.

To evaluate the validity of these approaches in this model, we consider directly the measured phase-space density, $\bar{f}(\epsilon)$, as a function of particle energy. To do so we measure the (averaged) values of the potential $\phi(x)$ and $a(\varphi)$ in the QSSs, and then use (17) to calculate the phase-space density $D(\epsilon)$. Shown in Fig. 19 are the results for eight chosen cases from the DRW initial conditions with $\xi_D = 0.56$ considered in Sec. V D. In Fig. 20 a plot of exactly the same data is given, but now displaying the logarithm of the absolute value of $\bar{f}/(f_0 - \bar{f})$ as a function of ϵ (which in LB theory gives a straight line with slope β). Our choice is representative of the whole batch of initial conditions, in that (1) most QSSs have a clear core-halo structure and (2) those that do not agree reasonably well with the LB prediction. Indeed the two configurations in the uppermost panel of Fig. 19 are the same two cases for which the full distribution functions were shown in Figs. 13 and 14.

In Fig. 19 a vertical line indicates the initial phase phase density f_0, so that it is clear that whenever a core appears it is indeed *degenerate*. While the measured phase-space

distributions are clearly more structured than (28), in most cases this simple ansatz gives a reasonably good fit (i.e., about as close to the phase-space density as the LB profile is to the observed one in the cases where it has been considered to work well above). The slightly greater structuration of the phase-space density compared to the ansatz of (28) can also be seen in Fig. 20, which shows in particular that the diffuse halo, when present, although close to flat, appears clearly more consistent with a Maxwell-Boltzmann form (i.e., the nondegenerate limit of LB theory). In this respect we note that Levin *et al.* have not tested their ansatz directly against the phase-space density, but have used it to derive predictions for $\rho(x)$ and $\theta(v)$, which have been compared with those observed. As we have seen in comparing numerical results with LB predictions above, these quantities typically wash out structure in energy space and make it difficult to see discrepancies that are localized in this space. We note further that our finding that it is initial conditions with $R_0 \approx 1$ that suppress the core-halo formation—and lead to QSSs in reasonable agreement with LB—appears completely coherent with the mechanism described by Levin *et al.*: When the system starts close to virial equilibrium, the relaxation is typically indeed much "gentler," simply because the system does not undergo the large contractions and expansions that result necessarily if there is a large imbalance between the initial potential and kinetic energy. It is precisely such macroscopic oscillations of the system that drive the resonances analyzed by Levin *et al.*

We consider finally comparison of our results with an analytical treatment of collisionless relaxation developed in Ref. [26] (see also references therein). This work develops, under certain approximations and hypotheses, a kinetic equation for collisionless relaxation—similar to the Lenard-Balescu equation for collisional relaxation—with a term describing relaxation toward the LB equilibrium. One feature of this term is that it involves an effective space and time-dependent diffusion coefficient, which is proportional to the product $\bar{f}(f_0 - \bar{f})$. Thus the theory suggests that relaxation should be expected to be most inefficient when $\bar{f}$ is close to degenerate ($\bar{f} \simeq f_0$) or very small ($\bar{f} \simeq 0$). In regions of energy where relaxation is more complete, the distribution is expected to approach the LB form, but with values of the parameters β and μ different from those in the global LB equilbrium. Our results in Figs. 19 and 20 do appear to be quite consistent with these qualitative predictions: Indeed, this theory would appear to account for why it is core-halo-type states, whose dynamical origin is explained by Levin *et al.*, that do not relax to the (global) LB equilibrium. In all cases the results in Fig. 20 show a region where the halo distribution is very consistent with a Maxwell-Boltzmann form with an inverse temperature lower than that of the global LB prediction (dashed line). This can be interpreted, following Ref. [26], as a "mixing region" where the (in this case, nondegenerate) LB distribution applies locally, while the deviation from the (local) LB form at higher and lower energies is considered as due to incompleteness of relaxation in these regions. Further, the fact that the observed distributions are, compared to the extrapolated straight line ("local" LB) fit in the"mixing region," sensibly higher at lower energies and lower at the highest energies is also in apparent agreement with the kinetic theory described in Ref. [26].

VII. CONCLUSION AND DISCUSSION

We summarize now our principal conclusions:

(1) *Attainment of QSSs in the SGS model:* In all cases we have considered QSSs do appear to be attained, but the time scales for relaxation to them can vary very considerably. In some cases rotating "holes" formed in the phase-space density during the initial phase of violent relaxation ($\sim 10^2 t_c$) survive for quite a long time, disappearing only on times scales of order ($\sim 10^3 t_c$). As on these latter time scales the system shows no apparent tendency to relax toward its thermodynamic equilibrium, we conclude that this is simply a manifestation of slow collisional relaxation and does not imply that QSSs are not attained as argued by Refs. [24,25]. A fuller study of the possible N dependence of such relaxation would be useful to establish this conclusion more firmly (but would be numerically challenging).

(2) *LB theory in the SGS model:* As was clear already from early studies [13,14], and confirmed by more recent ones such as Ref. [15], LB theory is not an adequate theory for understanding fully, or even approximately, the properties of QSSs arising from violent relaxation in the SGS model *for arbitrary initial conditions*. However, it is by no means an irrelevant theory to understanding these QSSs. Our study of a quite broad range of initial conditions shows that the space of QSSs in this model divides quite neatly into two: those for which LB works to quite a good approximation, and those for which the phase-space density is characterized by a degenerate core, taking a form generally quite close to the simple ansatz (28) proposed by Levin *et al.* The initial conditions in the former class are either close to the degenerate limit, or in other cases characterized by initial virial ratio of order unity. These conditions are precisely those, in line with what has been described by Levin *et al.,* that suppress resonances that otherwise act very efficiently to produce the degenerate core-halo structure.

(3) *Accuracy of predictions of QSSs in the SGS model:* While, as just described, the QSSs that result from violent relaxation divide into those that are close to the LB theory, on the one hand, or to the ansatz of Levin *et al.,* on the other, the accuracy of the associated predictions is at best approximate: *In no case* do we see a perfect agreement with either LB theory or the ansatz (28). We underline that in this respect the spatial distribution of mass $\rho(x)$ and velocity distribution $\theta(v)$ are rather poor tools for diagnosing the agreement between observations and theory, as they wash out deviations that are most pronounced in energy space. We have also noted the apparent coherence of our results with the qualitative predictions of the kinetic theory approach described in Ref. [26].

Numerous results in the literature on various other models (see references in introduction) for specific ranges of initial conditions suggest that these latter two conclusions, and probably the first also, might apply much more generally to long-range systems. Further detailed investigation of such models, and in particular of broader classes of waterbag initial conditions like those considered here, or, for example, "multilevel" waterbag initial conditions would be required to establish if this is the case.

For the SGS it would be interesting to apply the analysis described by Levin *et al.* to determine a prediction of the form

(28) for different initial conditions, and see how well it does in approaching the observed QSSs. In this respect it is interesting perhaps to note that, at given value of ξ_D this is a one parameter family of solutions, so that it predicts QSSs lying on a curve in the (ϕ_{11},ϕ_{22}) plane. In Fig. 10, we see that the QSSs obtained from the two-parameter family of initial conditions at a fixed $\xi_D = 0.56$ do approximately collapse onto a curve. We would expect the degree to which the simple ansatz (28) can fit the QSSs to be well characterized by determining the prediction it gives in this plane.

Of particular interest is of course the original context of 3D self-gravitating systems, to which the initial study of Ref. [8] for SRW suggests these conclusions may indeed apply. As mentioned, however, the results reported have been based, in this case, on examination of the density profile $\rho(x)$ alone, while the energy distribution is probably a finer diagnostic tool as we have seen here. In forthcoming work we will study this case and discuss the possible relevance of our findings in the astrophysical context. In this respect we note one of the reasons why LB theory has not played—at least for what concerns it detailed predictions—a role in astrophysics is that these predictions depend on unobservable initial phase-space densities. In contrast the prediction of a degenerate core in many cases would give a simple link between observations and initial conditions, which may be of practical relevance notably in constraining the parameters in theories of structure formation in the universe.

ACKNOWLEDGMENTS

The simulations were carried out in large part at the Centre de Calcul of the Institut de Physique Nucléaire et Physique des Particules. We are particularly grateful to Laurent Le Guillou for advice and help on use of these computing resources. We thank B. Marcos for useful discussions, and P. H. Chavanis for many helpful remarks, and in particular for suggesting the plot in Fig. 20.

APPENDIX A: DETERMINATION OF β AND μ

In general β and μ cannot be calculated analytically, so we solve for them numerically as follows. The mass normalization (4) condition is

$$M = \int_{-\infty}^{\infty}\int_{-\infty}^{\infty} \bar{f}(x,v)\,dx\,dv.$$

Integrating over v, and changing the coordinate x to $\varphi(x)$ just as in (8), we obtain

$$M = 4\int_0^{\infty}\int_0^{\infty} \frac{\bar{f}(\varphi,v)}{a(\varphi)}\,dv\,d\varphi. \tag{A1}$$

The total energy constraint (5), i.e.,

$$E = \int_{-\infty}^{\infty}\int_{-\infty}^{\infty}\left[\frac{v^2}{2}+\frac{\varphi(x)}{2}\right]\bar{f}(x,v)\,dx\,dv,$$

can likewise be rewritten as

$$\begin{aligned} E &= 2\int_0^{\infty}\int_0^{\infty}\frac{v^2\bar{f}(\varphi,v)}{a(\varphi)}\,dv\,d\varphi \\ &\quad + 2\int_0^{\infty}\int_0^{\infty}\frac{\varphi\bar{f}(\varphi,v)}{a(\varphi)}\,dv\,d\varphi \\ &= T+U, \end{aligned} \tag{A2}$$

where T is total kinetic energy and U is total potential energy. We can then use the virialization condition, $2T = U$, to obtain

$$E = 6\int_0^{\infty}\int_0^{\infty}\frac{v^2\bar{f}(\varphi,v)}{a(\varphi)}\,dv\,d\varphi. \tag{A3}$$

The determination of the parameters β and μ in the LB solution (3) can then be cast as the problem of finding the solutions of the equations

$$\begin{aligned} F(\beta,\mu) &= 0, \\ G(\beta,\mu) &= 0, \end{aligned}$$

where

$$F(\beta,\mu) = M - 4\int_0^{\infty}\int_0^{\infty}\frac{f_0}{1+e^{\beta\left(\frac{v^2}{2}+\varphi-\mu\right)}}\frac{1}{a(\varphi)}\,dv\,d\varphi, \tag{A4}$$

$$G(\beta,\mu) = E - 6\int_0^{\infty}\int_0^{\infty}\frac{v^2 f_0}{1+e^{\beta\left(\frac{v^2}{2}+\varphi-\mu\right)}}\frac{1}{a(\varphi)}\,dv\,d\varphi. \tag{A5}$$

Following a standard method we write the matrix equation

$$\begin{pmatrix} dF(\beta,\mu) \\ dG(\beta,\mu)\end{pmatrix} = \begin{pmatrix} \frac{\partial F}{\partial\beta} & \frac{\partial F}{\partial\mu} \\ \frac{\partial G}{\partial\beta} & \frac{\partial G}{\partial\mu}\end{pmatrix}\begin{pmatrix} d\beta \\ d\mu\end{pmatrix}, \tag{A6}$$

where dF and dG denote the infinitesimal changes of F and G when (β,μ) change to $(\beta+d\beta,\mu+d\mu)$, we start by guessing a pair of (β,μ) and then determining the new $(\beta',\mu') = (\beta+\Delta\beta,\mu+\Delta\mu)$ using

$$\begin{pmatrix} \Delta\beta \\ \Delta\mu\end{pmatrix} = \begin{pmatrix} \frac{\partial F}{\partial\beta} & \frac{\partial F}{\partial\mu} \\ \frac{\partial G}{\partial\beta} & \frac{\partial G}{\partial\mu}\end{pmatrix}^{-1}\begin{pmatrix} \Delta F(\beta,\mu) \\ \Delta G(\beta,\mu)\end{pmatrix}, \tag{A7}$$

where $(\Delta F,\Delta G) = [-F(\beta,\mu), -G(\beta,\mu)]$. We then iterate until ΔF and ΔG converge to 0. With a reasonable guess for the starting values of β and μ, good convergence is attained within a few iterations, as illustrated in Fig. 21 for a typical case.

APPENDIX B: DEGENERATE LIMIT OF LB THEORY

For completeness we reproduce here the analytic results of [14] (see also Ref. [29]) for the degenerate limit of the LB distribution function (3). This corresponds to $\beta\to\infty$, in which

$$f(x,v) = \begin{cases} f_0, & \epsilon(x,v) < \mu \\ 0, & \text{otherwise.}\end{cases} \tag{B1}$$

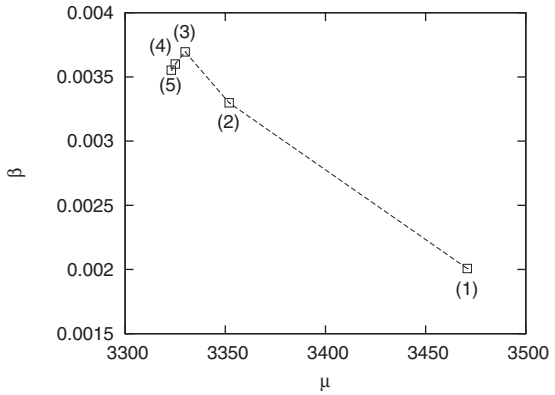

FIG. 21. The values of β and μ obtained in the successive steps of our iterative numerical calculation, for a typical case. The units here are those used in our numerical calculation ($M = N$, $g = 1$ and $L_0 = N$), different from those in which our results in the main text are given.

The density profile is then

$$\rho(\varphi) = 2\int_0^{\sqrt{2(\mu-\varphi)}} f_0\, dv = 2\sqrt{2} f_0 (\mu-\varphi)^{\frac{1}{2}}, \tag{B2}$$

and therefore, using (11),

$$a(\varphi) = 4 \times 2^{\frac{1}{4}} \times \left(\frac{g f_0}{3}\right)^{\frac{1}{2}} \left[\mu^{\frac{3}{2}} - (\mu-\varphi)^{\frac{3}{2}}\right]^{\frac{1}{2}}. \tag{B3}$$

The mass normalization then yields

$$M = 2\int_0^{\mu} \frac{\rho(\varphi)}{a(\varphi)}\, d\varphi = \frac{4\sqrt{2} f_0}{\sqrt{\frac{16\sqrt{2} g f_0}{3}}} \int_0^{\mu} \frac{(\mu-\varphi)^{\frac{1}{2}}\, d\varphi}{\left[\mu^{\frac{3}{2}} - (\mu-\varphi)^{\frac{3}{2}}\right]^{\frac{1}{2}}} = 2^{\frac{5}{4}} \left(\frac{f_0}{3g}\right)^{\frac{1}{2}} \int_{\varphi=0}^{\varphi=\mu} \frac{d\left[\mu^{\frac{3}{2}} - (\mu-\varphi)^{\frac{3}{2}}\right]}{\left[\mu^{\frac{3}{2}} - (\mu-\varphi)^{\frac{3}{2}}\right]^{\frac{1}{2}}},$$

which can be integrated to give

$$M = 2^{\frac{9}{4}} \left(\frac{f_0}{3g}\right)^{\frac{1}{2}} \mu^{\frac{3}{4}}. \tag{B4}$$

Using the expression (A3) for the total energy we have

$$E_D = 6 f_0 \int_0^{\mu} \int_0^{\sqrt{2(\mu-\varphi)}} \frac{v^2}{a(\varphi)}\, dv\, d\varphi.$$

Integration first over v gives

$$E_D = 2^{\frac{1}{4}} \left(\frac{3 f_0}{g}\right)^{\frac{1}{2}} \int_0^{\mu} \frac{(\mu-\varphi)^{\frac{3}{2}}}{\left[\mu^{\frac{3}{2}} - (\mu-\varphi)^{\frac{3}{2}}\right]^{\frac{1}{2}}}\, d\varphi,$$

and then, on integrating by parts, we obtain

$$E_D = \frac{2^{\frac{13}{4}}}{3} \left(\frac{f_0}{3g}\right)^{\frac{1}{2}} \mu^{\frac{7}{4}} \int_0^1 (1-\varphi')^{\frac{1}{2}} \varphi'^{-\frac{1}{3}}\, d\varphi',$$

where $\varphi' = (\frac{\mu-\varphi}{\mu})^{\frac{3}{2}}$. The integral can be expressed as a beta function, and the result can thus be written

$$E_D = \frac{2^{\frac{13}{4}}}{3} \left(\frac{f_0}{3g}\right)^{\frac{1}{2}} B\left(\frac{3}{2}, \frac{2}{3}\right) \mu^{\frac{7}{4}}. \tag{B5}$$

It is simple to show from (A2) that $\frac{\partial E}{\partial \beta} < 0$ in general, tending asymptotically to 0 as $\beta \to \infty$. This is thus, indeed, the minimal possible energy corresponding to given M and f_0.

APPENDIX C: GENERATION OF DRW INITIAL CONDITIONS

For the DRW phase-space density defined in Sec. II a direct calculation gives immediately that the initial kinetic energy is

$$T_0 = f_0 \left[\frac{2(x_2 - x_1) v_2^3}{3} + \frac{2 x_1 v_1^3}{3}\right],$$

and the initial potential energy

$$U_0 = 4 f_0^2 v_2^2 g \left[\frac{4x_2^3}{3} + \frac{2x_1^3}{3} - 2x_2^2 x_1\right] + 8 f_0^2 v_1 v_2 g \left[x_1\left(x_2^2 - x_1^2\right)\right] + \frac{16}{3} f_0^2 v_1^2 g x_1^3.$$

These indeed reduce to the corresponding expressions (23) for the SRW (when we set $x_1 = 0$, $x_1 = x_2$ or $v_1 = v_2$). To generate the specific initial condition reported in Sec. V D, we do a random sampling in in x_1, x_2, v_1, and v_2 at fixed f_0, E and M fixed (which implies that ξ_D is fixed). We then choose configurations with $R_0 = 2T_0/U_0$ and δ as various as possible.

[1] A. Campa, T. Dauxois, and S. Ruffo, Phys. Rep. **480**, 57 (2009).
[2] D. Lynden-Bell, Mon. Not. R. Astron. Soc. **136**, 101 (1967).
[3] P. H. Chavanis, J. Sommeria, and R. Robert, Astrophys. J. **471**, 385 (1996).
[4] A. Antoniazzi, D. Fanelli, J. Barre, P. H. Chavanis, T. Dauxois, and S. Ruffo, Phys. Rev. E **75**, 011112 (2007).
[5] F. Staniscia, P. H. Chavanis, G. De Ninno, and D. Fanelli, Phys. Rev. E **80**, 021138 (2009).
[6] S. Tremaine, M. Henon, and D. Lynden-Bell, Mon. Not. R. Astron. Soc. **219**, 285 (1986).
[7] I. Arad and D. Lynden-Bell, Mon. Not. R. Astron. Soc. **361**, 385 (2005).
[8] Y. Levin, R. Pakter, and F. B. Rizzato, Phys. Rev. E **78**, 021130 (2008).
[9] Y. Levin, R. Pakter, and T. N. Teles, Phys. Rev. Lett. **100**, 040604 (2008).
[10] T. N. Teles, Y. Levin, R. Pakter, and F. B. Rizzato, J. Stat. Mech. Theor. Exp. (2010) P05007.
[11] R. Pakter and Y. Levin, e-print arXiv:1012.0035 (2010).
[12] F. Hohl and J. Campbell, Astron. J. **73**, 611 (1968).

[13] S. Goldstein, S. Cuperman, and M. Lecar, Mon. Not. R. Astron. Soc. **143**, 209 (1969).
[14] M. Lecar and L. Cohen, Astrophys. Space Sci. **13**, 397 (1971).
[15] Y. Yamaguchi, Phys. Rev. E **78**, 041114 (2008).
[16] G. L. Camm, Mon. Not. R. Astron. Soc. **110**, 305 (1950).
[17] G. Rybicki, Astrophys. Space Sci. **14**, 56 (1971).
[18] T. Tsuchiya, N. Gouda, and T. Konishi, Phys. Rev. E **53**, 2210 (1996).
[19] B. N. Miller, Phys. Rev. E **53**, R4279 (1996).
[20] K. R. Yawn and B. N. Miller, Phys. Rev. E **68**, 056120 (2003).
[21] M. Joyce and T. Worrakitpoonpon, J. Stat. Mech. Theor. Exp. (2010) P10012.
[22] P.-H. Chavanis, J. Stat. Mech. Theor. Exp. (2010) P05019.
[23] Y. Yamaguchi, J. Barre, F. Bouchet, T. Dauxois, and S. Ruffo, Physica A **337**, 36 (2004).
[24] P. Mineau, M. R. Feix, and J. L. Rouet, Astron. Astrophys. **228**, 344 (1990).
[25] J. L. Rouet and M. Feix, Phys. Rev. E **59**, 73 (1999).
[26] P. H. Chavanis, Physica A **387**, 1504 (2008).
[27] A. Noullez, E. Aurell, and D. Fanelli, J. Comput. Phys. **186**, 697 (2003).
[28] M. Luwel, G. Severne, and P. Rousseeuw, Astrophys. Space Sci. **100**, 261 (1984).
[29] P.-H. Chavanis, Phys. Rev. E **69**, 066126 (2004).